



# Modelling transient thermal processes in the lithosphere: application to the NW Pannonian basin

Eszter Békési<sup>1</sup>, Jan-Diederik van Wees<sup>2</sup>, Kristóf Porkoláb<sup>1</sup>, Mátyás Hencz<sup>1</sup>, Márta Berkesi<sup>1</sup>

<sup>1</sup>MTA-EPSS Lendület (Momentum) FluidsByDepth Research group, HUN-REN Institute of Earth Physics and Space Science,  
5 9400 Sopron, Hungary

<sup>2</sup>TNO Utrecht, Utrecht 3584 CB, Netherlands

*Correspondence to:* Eszter Békési (bekesi.eszter@epss.hun-ren.hu)

**Abstract.** The reconstruction of thermal evolution in sedimentary basins is a key input for constraining geodynamic processes and geo-energy resource potential. We present a methodology to reproduce the most important transient thermal footprints  
10 accompanying basin formation: lithosphere extension and sedimentation. The forward model is extended with data assimilation to constrain models with temperature measurements. We apply the methodology to the NW part of Hungary. Realistic past- and present-day temperature predictions for the entire lithosphere are achieved, suggesting the relatively uniform, but strong attenuation of the mantle lithosphere through extension, and relatively small variations in the present-day thermal lithosphere thickness. The new temperature model allows an improved estimation of lithosphere rheology and the interpretation of mantle  
15 xenolith origins.

## 1 Introduction

Understanding the thermal state and thermal evolution of the lithosphere of sedimentary basins are crucial both for constraining fundamental geodynamic, geological, and geochemical processes and observations on lithosphere scale, as well as for geo-energy perspectives such as geothermal and hydrocarbon exploration and resource characterization. Sedimentary basins,  
20 through their formation, exhibit a typical thermal evolution pattern. During the active rifting phase, surface heat flow, lithosphere temperature and geothermal gradient rise, governed by the thinning of the lithosphere and consequent rise of the asthenosphere (e.g. Buck et al., 1988). Subsequently, the thermal relaxation of the lithosphere begins through conductive cooling and thermal subsidence. The duration of both the syn- and post rift phases vary significantly, however, reaching equilibrium (steady-state) typically takes several tens to hundreds of million years (Van Wees et al., 2009; Xie and Heller,  
25 2009; Petersen et al., 2015).

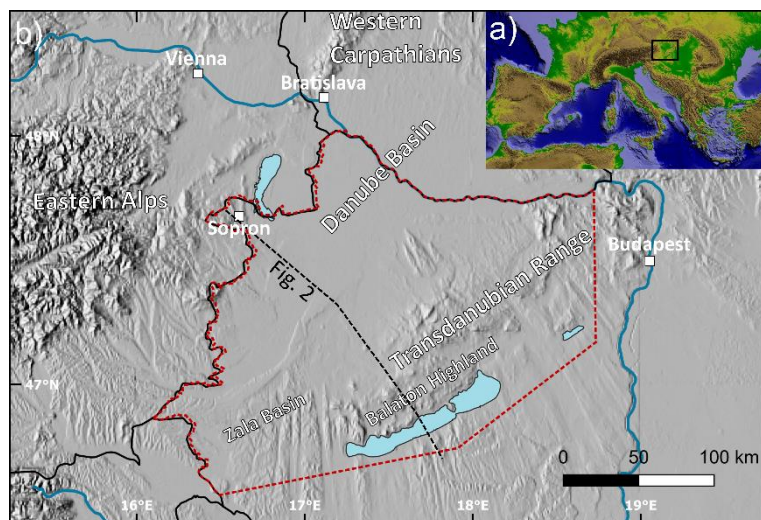
Thermo-mechanical numerical models can provide past and present-day temperature predictions where thermal and mechanical processes are coupled. In contrast, purely thermal calculations can only incorporate mechanical effects of lithosphere extension through modelling its thermal footprint, by tectonic heat flow calculations based on stretching models such as McKenzie (1978), Royden and Keen (1980). One limitation of thermo-mechanical models for the prediction of  
30 lithosphere temperatures and thermal evolution is the commonly lower resolution and less detailed lithological subdivision in the upper crust, which has very important control on the shallow temperature field. Additionally, thermo-mechanical models

do not allow for the incorporation of temperature observations. Forward modelling workflows are not capable of constraining model parameters with measurement data, resulting in a limited applicability of modelled temperatures for geothermal exploration.

35 In this paper we present a new methodology that accounts for the most important thermal effects that accompany basin formation such as lithosphere extension, sedimentation/erosion, and changes in thermal properties, most importantly the radiogenic heat generation in upper crust, largely building on the methodology of Van Wees et al. (2009). The transient thermal modelling workflow is extended with a data assimilation framework to constrain model parameters with present-day temperature observations, that allows the validation of the resulting model predictions. We demonstrate and apply the new  
40 methodology to the NW part of the Pannonian basin (Fig. 1).

The Pannonian basin exhibits an attenuated crust and lithosphere (Hetényi and Bus, 2007; Kalmár et al., 2021; Kalmár et al., 2023) and therefore high heat flow (an average of 90 mW/m<sup>2</sup>) and geothermal gradient (an average of 45 °C/km), constituting one of the hottest basins in Europe (Lenkey et al., 2002; Békési et al., 2018; Horváth et al., 2015; Limberger et al., 2018). Lithosphere extension in the Pannonian basin took place in the Early–Middle Miocene migrating from NW towards SE.  
45 Consequently, surface heat flow and geothermal gradient in the NW part of the basin constituting the study area is generally lower, but the thermal footprint of extension is still notable. Extension was followed by post-rift cooling and subsidence accompanied by contractional basin inversion from the Late Miocene (e.g. Balázs et al., 2016; Fodor et al., 2005; Horváth and Cloetingh, 1996; Tari, 1994; Tari et al., 2020) to present day (Grenerczy et al., 2005; Bada et al., 2007; Porkoláb et al., 2023; Békési et al., 2023). Despite the inversional overprint, the thermal footprint of Miocene lithosphere extension is still the most  
50 important factor that determines the present-day thermal state of the lithosphere. Consequently, the past and present-day temperature distribution in the lithosphere can only be fully captured by modelling the transient thermal effect of syn-rift extension and post-rift cooling, accompanied by changes in lithosphere structure and thermal properties (i.e. compositional changes through sedimentation, upper crustal radiogenic heat generation).

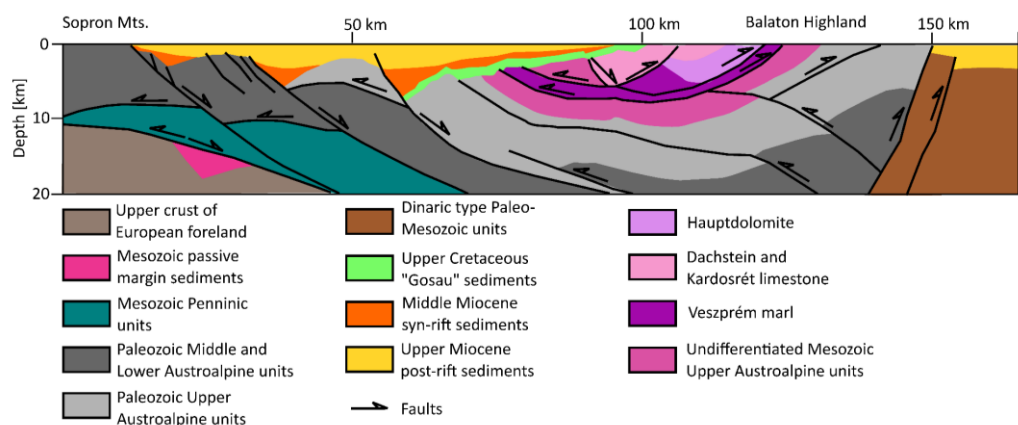
Physics-based thermal models constructed for (parts of) the Pannonian basin mainly focused on the representation of the  
55 temperature distribution within the upper crust, providing boundary conditions for geothermal exploration (Lenkey et al., 2017; Békési et al., 2018). Such models were constructed either without performing actual transient calculations (Békési et al., 2018) or were not conditioned by temperature measurements (only the forward modelling exercise was performed (Lenkey et al., 2017)). We aim to provide temperature predictions that can further improve on existing models to represent past and present-day temperature distribution within the whole lithosphere with high precision. We discuss some important implications to the  
60 thermal evolution of the region, as well as to the rheology of the lithosphere. Moreover, we outline its applications for geochemical measurements on xenoliths.



65 **Figure 1: a) Topographic map of Europe based on the SRTM digital elevation model (Farr et al., 2007) , showing the outline of Fig. 1b (black rectangle) b) Geography of the study area based on the GMTED2010 elevation model (Danielson and Gesch, 2011). Red polygon denotes the extent of the thermal model, black lines denote state borders.**

## 2 Geological setting

Our study area in NW-Hungary comprises sub-basins of the Miocene Pannonian basin system (Danube basin, Zala basin) and the Transdanubian Range, where the pre-Cenozoic basement units outcrop over a hilly region (Figs. 1, 2). The Danube basin (also called Little Hungarian Plain) is one of the deepest (up to 9 km (Kilényi and Šefara, 1989)) sub-basins of the Pannonian basin and is framed by the Eastern Alps to the west, the Western Carpathians to the north, and the Transdanubian Range to the southeast. The sedimentary succession of the Danube basin overlies an Alpine nappe stack of basement units consisting of Adria-derived thrust sheets (Austroalpine nappe system), remnants of the Alpine Tethys ocean (Penninic nappe), and units of the lower plate (Europe-derived units). During the Miocene opening of the Danube basin, normal faults partially reactivated and partially cut through the Alpine nappe contacts in the basement (Tari et al., 2021). The Alpine nappe stack is exposed on the NW and SE margins of the Danube basin: the Lower Austroalpine nappe in the Sopron Mountains, while the Upper Austroalpine units in the Transdanubian Range (Fig. 2 (Tari, 1994; Schmid et al., 2008)). The Transdanubian Range exhibits a thick Mesozoic platform carbonate succession (Fig. 2) that defines its characteristic thermal properties (Table 1) and typical karstic hydrology (Mádl-Szőnyi and Tóth, 2015).



80 **Figure 2: Geological cross section through the study area (for location see Fig. 1) showing the most important regional units and faults, modified after Szafián et al. (1999).**

### 3 Data and methods

#### 3.1 Model geometry and thermal properties

85 The temperature model extends to the whole lithosphere in the NW part of the Pannonian basin, restricted to its Hungarian part. Restricting the model area to the Hungarian part was necessary due to the availability of geological horizons and temperature measurements. The model was built in the Hungarian coordinate system (HD72 / EOV) with a horizontal resolution of ~ 3 km and a vertical resolution of 200 m for the uppermost 5 km and 2.5 km down to 120 km depth, which was selected as the bottom of the lithosphere prior to extension.

90 The model is built up by the present configuration of sedimentary layers, upper crust, lower crust, and lithospheric mantle. The sediments were subdivided into four layers; Quaternary, Upper Pannonian (Upper Miocene post-rift), Lower Pannonian (Upper Miocene post-rift), and pre-Pannonian Neogene (Middle-Miocene syn-rift) units built up by the mixture of clastic sediments (Table 1). For the geometry of the pre-Cenozoic basement, we adopted the basement map of Haas et al. (2014). We included an additional layer for the Mesozoic carbonate basement units, since they constitute relatively thick (up to a few kms) successions throughout parts of the study area and have significantly different thermal properties compared to crystalline  
 95 basement units. We constructed a thickness map for the carbonates based on published cross-sections (Budai et al., 1999; Szafián et al., 1999; Héja et al., 2022). For the depth of the lower and upper crust in the present-day model, we used the most recent crustal models constructed from seismological observations (Kalmár et al., 2021). Except for the starting model for the time dependent calculations (representing the thermal state of the lithosphere prior to extension), we allowed the lithospheric mantle to stretch with a spatially variable factor (subcrustal stretching factor, see section 3.3) instead of using any present-day  
 100 lithospheric thickness maps. The depth of the lithosphere-asthenosphere boundary (LAB) prior to stretching was set to a constant 120 km, and the initial crustal thickness was set to 35 km.



We calculated the thermal conductivities of the layers using thermal and petrophysical parameters of typical lithotypes after Hantschel and Kauerauf (2009). In case of the sedimentary units, we modified the parameters of lithotypes listed in Hantschel and Kauerauf (2009) based on the thermal conductivity empirical formulas for clastic sediments (pelites and psammities) in the Pannonian basin (Dövényi and Horváth, 1988). Since each sedimentary layer and the carbonate layer are built up by various lithotypes, the bulk rock matrix thermal conductivities were calculated by taking the harmonic mean of the individual matrix thermal conductivities of the lithotypes. The sediment bulk thermal conductivities were finally obtained using the geometric mean of the bulk matrix conductivities and the thermal conductivity of the pore fluid. Typical thermal conductivity values of the upper and lower crust and lithospheric mantle were corrected for pressure- and temperature conditions based on Chapman (1986) in case of the crust, and Schatz and Simmons (1972) and Xu et al. (2004) for the mantle lithosphere. The detailed calculation of the thermal conductivities is described in (Limberger et al., 2018) and ranges of thermal conductivity values of the layers are listed in Table 1.

Similar to the thermal conductivities of the sedimentary units and the carbonate layer, radiogenic heat generation of each layer was calculated as a mixture of typical values of lithotypes (Hantschel and Kauerauf, 2009), corrected for compaction (values in sediments generally increase with depth due to decreasing porosity). The radiogenic heat generated in the granitic upper crust is generally considerably larger than in case of sedimentary, lower crustal and lithospheric mantle units. Therefore, it was increasingly important to distinguish the carbonate and crystalline basement units for the proper prediction of upper crustal temperatures. Although, the radiogenic heat generation of compacted shale layers is in the order of magnitude of the upper crust, therefore, maximum values of the sediment heat generation corresponding to the deep Lower Pannonian shales is up to 1.7  $\mu\text{W}/\text{m}^3$  (Table 1). The radiogenic heat generation of the crust and lithospheric mantle were selected to constants. For the upper crust, we chose a typical continental upper crustal heat generation value of 1.4  $\mu\text{W}/\text{m}^3$ , while the lower crustal and mantle lithosphere heat generation was selected to 0.4  $\mu\text{W}/\text{m}^3$  and 0.002  $\mu\text{W}/\text{m}^3$  based on Hantschel and Kauerauf (2009) (Table 1).

Layer name	Lithology	Thermal conductivity [W/m*K]	Radiogenic heat production [ $\mu\text{W}/\text{m}^3$ ]
Quaternary	70% sand; 30% shale	Bulk values per lithotypes (mixed lithologies) based on Hantschel and Kauerauf (2009) and Dövényi and Horváth (1988), dependent on compaction and temperature; ranging between 1.2-2	Bulk values per lithotypes based on Hantschel and Kauerauf (2009) dependent on compaction; ranging between 0.4-1.7
Upper Pannonian (Upper Miocene)	50% sand; 50% shale		
Lower Pannonian (Upper Miocene)	10% sand; 90% shale		



Neogene (pre-Pannonian)	70% sand; 30% conglomerate		
Mesozoic carbonate	30% limestone; 60% dolomite; 10% sand	Bulk values per lithotypes (mixed lithologies) based on Hantschel and Kauerauf (2009) dependent on compaction and temperature; ranging between 1.8-2.8	Bulk values per lithotypes based on Hantschel and Kauerauf (2009) dependent on compaction; ranging between 0.3-0.4
Upper crust	100% granite	Bulk values per lithotypes (Hantschel and Kauerauf, 2009) corrected for pressure and temperature (Chapman, 1986); ranging between 2-2.8	Constant based on Hantschel and Kauerauf (2009); 1.4
Lower crust	100% granulite		Constant based on Hantschel and Kauerauf (2009); 0.5
Mantle lithosphere	100% peridotite	Bulk values per lithotypes (Hantschel and Kauerauf, 2009) corrected for pressure and temperature (Schatz and Simmons, 1972; Xu et al., 2004), ranging between 2.8-3.5	Constant based on Hantschel and Kauerauf (2009); 0.02

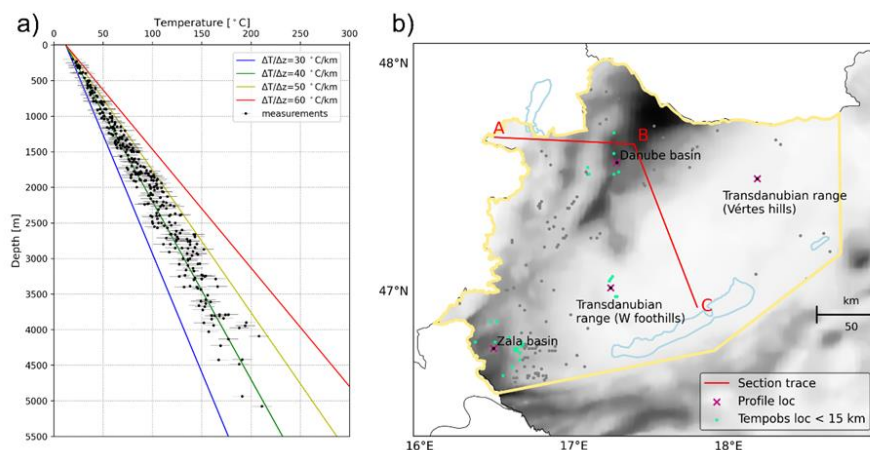
125 **Table 1: Lithology and thermal properties of model layers.**

### 3.2 Temperature observations and data uncertainties

We calibrated the thermal model with subsurface temperature measurements from hydrocarbon and geothermal wells. Measurements from the Geothermal Database of Hungary (Dövényi and Horváth, 1988; Dövényi et al., 2002) the Geothermal Information System (Ogre, 2020) were collected, including bottom hole temperatures (BHTs), drill-stem tests (DSTs), steady-  
 130 state temperature logs and outflowing water temperatures from geothermal wells. Temperature measurements were carefully reviewed and observations from areas where the conductive thermal field is strongly influenced by fluid flow and observations with errors larger than 10 °C were excluded from the dataset. This was necessary as the model, focusing primarily on lithosphere-scale processes, could not account for convective heat transfer, and temperature measurements influenced by fluid



135 flow would have biased the predicted lithosphere temperatures. The resulting number of temperature observations used for calibration was 335, covering the depth interval of 200-5100 (Figure 3a). Measurements are not evenly distributed throughout the study area; most of them are available from basinal locations (Figure 3b). Observations from the vicinity of the Transdanubian range are rather limited due to the presence of regional deep fluid pathways (Mádl-Szönyi and Tóth, 2015; Tóth et al., 2023) and resulting convective thermal field, also evidenced by the low surface heat flow due to the infiltration of cold meteoric water (Lenkey et al., 2002).



140

**Figure 3:** (a) Temperature dataset used for the calibration of the thermal model. Temperature measurements were obtained from the Geothermal Database of Hungary (Dövényi and Horváth, 1988; Dövényi et al., 2002) and the Geothermal Information System (Ogre, 2020). Colours represent geotherms between 30 °C/km to 60 °C/km. (b) Locations of temperature measurements (grey, green and black circles), and locations of temperature profiles and section shown in Figs. 7-9, plotted on top of the pre-Cenozoic basement map (Haas et al., 2014).

145

We assigned errors to the temperature measurements according to (Békési et al., 2018; Békési et al., 2020). Symmetrical uncertainties were chosen for the measurements, between  $\pm 5$  to  $\pm 10$  °C, and uncertainties were selected identical for the same measurement types for simplicity. DSTs and outflow temperatures were marked by uncertainties of  $\pm 5$  °C, while for BHTs, generally having larger uncertainties (Goutorbe et al., 2007), a maximum error of  $\pm 10$  °C was chosen. For the remaining temperature measurements, we adopted the errors reported in the Geothermal Database of Hungary (Dövényi and Horváth, 1988; Dövényi et al., 2002).

150

Temperature measurements selected for calibration mostly scatter around the 40 °C/km geotherm (Fig. 3a), while several observations, both in shallower and deeper intervals, approximate the 50 °C/km geotherm. The overall geothermal gradient of the temperature dataset is 42 °C/km, which is slightly below the average geothermal gradient for the central part of the Pannonian basin ( $\sim 45$  °C/km), although much higher than average continental values, representing the thermal effect of the thinned lithosphere in the study area.

155



### 3.3 Forward model

The modelling procedure consists of three main steps, including steady-state conductive forward model calculations, transient calculations incorporating the thermal effect of lithosphere-scale processes, and the inversion procedure, when selected model parameter(s) are updated to decrease misfits between measured and modelled temperatures. In the first step, we calculated the thermal field prior to lithosphere extension (Section 3.3.1). In the second step, we used crustal and subcrustal stretching factors and sedimentation rates to account for the effects of lithosphere extension and subsequent cooling, as well as syn- and post-rift sedimentation (Section 3.3.2) damping of the thermal footprint of extension. The third step concerns the inversion workflow (Section 3.4), incorporating temperature measurements into the model as target observations to constrain the amount of lithosphere attenuation and as a result obtain more realistic temperature estimates during and after rifting.

#### 3.3.1 Steady-state calculations

The steady-state modelling approach provides initial conditions for the transient model calculations, by solving the heat equation for conduction in 3D:

$$0 = \nabla \cdot (\lambda \nabla T) + A \quad (1)$$

where  $\lambda$  is the thermal conductivity [ $\text{Wm}^{-1} \text{K}^{-1}$ ],  $T$  [K or  $^{\circ}\text{C}$ ] is the temperature,  $A$  is the radiogenic heat production [ $\text{Wm}^{-3}$ ], and  $\nabla = \left( \frac{\partial}{\partial x}, \frac{\partial}{\partial y}, \frac{\partial}{\partial z} \right)$  is the nabla operator. Equation (1) is solved numerically by a finite-difference approximation using the Preconditioned Conjugate Gradient method. Temperature boundary conditions on the top and bottom of the model were selected as  $12^{\circ}\text{C}$  and  $1330^{\circ}\text{C}$ , respectively. The top boundary condition of  $12^{\circ}\text{C}$  was selected as a mean surface temperature. The depth of the bottom boundary condition was selected to 120 km, which was assumed to be the depth of the LAB prior to lithosphere extension. The vertical edges of the model were assumed to be insulating with a fixed heat flow of zero. These boundary conditions remained active also for the transient model calculations both with and without incorporating the data assimilation procedure, since the steady-state model provided the initial setting of the transient modelling. Please note that the steady state geotherm is based on the present day (actual) crustal and sediment configuration in target prediction time (present day). As demonstrated in Van Wees et al. (2009) in high resolution 1D simulations, the steady state solution at production time target, corrected for transient effects related to kinematic effects of lithosphere deformation, and sedimentation provide a reliable thermal solution for in particular in the top 5-10 km of the model.

#### 3.3.2 Transient calculations

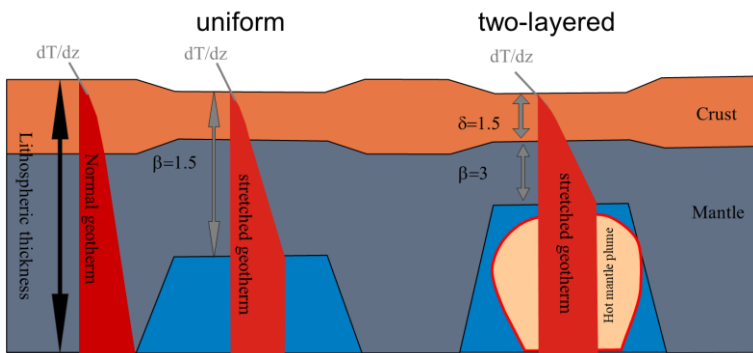
To correct the steady state solution (Equation 1) for transient effects, the thermal effects of lithosphere extension was incorporated in the model by integrating over simulation time for:





$$\frac{\partial T}{\partial t} = 1/\rho c_t \cdot [\nabla \cdot (\lambda \nabla T) + A] - v_z dT/dz \quad (2)$$

185 where  $t$  is time [s],  $\rho$  is density [ $\text{kgm}^{-3}$ ],  $c_t$  is specific heat capacity [ $\text{J kg}^{-1} \text{K}^{-1}$ ],  $v_z$  is vertical velocity of the sediment, crust and mantle in the Eulerian finite difference framework as a function of the tectonic stretching and sedimentation (cf. Van Wees et al., 2009; Bonté et al., 2012; Corver et al., 2009). The transient term was estimated based on crustal ( $\delta$ ) and subcrustal ( $\beta$ ) stretching factors and accounting for sedimentation, based on Van Wees et al. (2009). Crustal and subcrustal stretching factors represent the ratio between the initial and thinned crustal thickness and mantle lithosphere thickness, respectively, with values  
 190  $>1$  (e.g. Royden and Keen, 1980). For instance, in case of an initial crustal thickness of 30 km, and a thinned crustal thickness of 20 km,  $\delta$  equals to 1.5 (Fig. 4).



195 **Figure 4: Cartoon illustrating the crustal ( $\delta$ ) and subcrustal ( $\beta$ ) stretching factors.  $dT/dz$  represents the temperature gradient with depth showing a disturbed geotherm in the stretched part of the model. Non-uniform stretching of the crust and mantle lithosphere (with or without the presence of mantle plumes) can be accounted for by  $\beta > \delta$  after Van Wees et al. (2009) and Corver et al. (2009).**

The main extensional phase is dated to considerably different times in parts of the study area. Highest rates in the Zala basin are inferred between 19-15 Ma, while in western part of the Transdanubian Range active normal faulting started only at ~15 Ma and persisted until 8 Ma (Fodor et al., 2021). In the Danube basin, the syn-rift phase was active between ~16-10 Ma (Šujan et al., 2021). In the thermal model, we assumed a uniform timing for active rifting in the whole study area for simplicity, which  
 200 took place between 18-10 Ma (Table 2). It was necessary to later invert for subcrustal stretching factors in one step. For this period, we also considered sedimentation corresponding to the deposition of Pre-Pannonian Neogene sediments (Table 2).

Tima [Ma]	Initial crustal thickness [km]	Initial LAB depth [m]	Crustal stretching ( $\delta$ ) [-]	Subcrustal stretching ( $\beta$ ) [-]	Sedimentation [km]
18 — 10	35	120	Spatially variable calculated from the initial and present-day Moho depth and	Constant value of 3	Neogene (pre-Pannonian) sediment



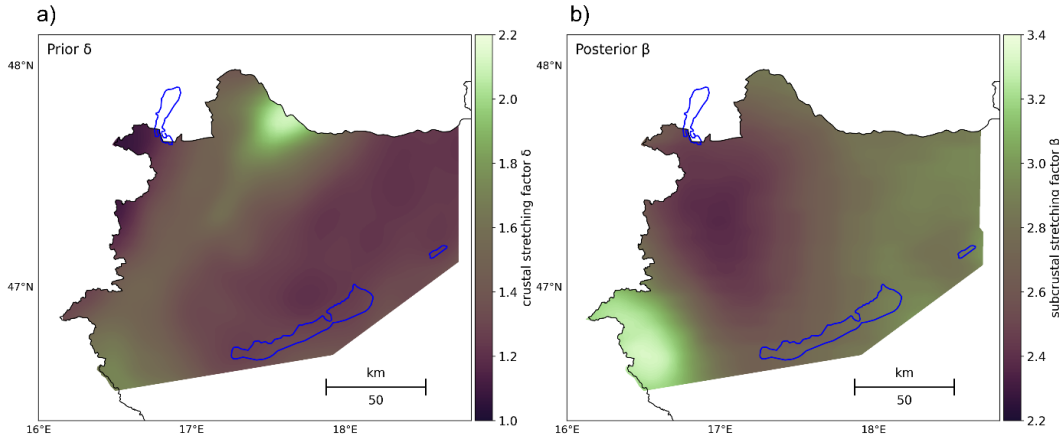
			basement depth, ranging between ~1 to 2.2		thickness, ranging between ~0-5
10 — 0	-	-	1	1	Pannonian and Quaternary sediment thickness, ranging between ~0-5

**Table 2: Input parameters of the stretching module.**

During the active rifting phase, we calculated the transient thermal effect of extension using crustal ( $\delta$ ) and subcrustal ( $\beta$ ) stretching factors for the area. Lenkey (1999) calculated these factors for the entire Pannonian basin, although after testing them we decided not to use them, primary due to the low  $\beta$  values predicted for the Transdanubian Range, resulting in unrealistically low past-extension temperatures in the area. We calculated new crustal stretching values similar to the methodology without heat flow observations described in Lenkey (1999) but based on the most recent present-day Moho depth of Kalmár et al. (2021) ( $Z_{Moho\ present}$ ). To be able to compare the new  $\delta$  grid with the earlier work of Lenkey (1999), we chose an initial crustal thickness ( $Z_{crust\ init}$ ) of 35 km. We calculated the present-day crustal thickness using the present-day basement depth (Haas et al., 2014). The equation for the crustal stretching factor  $\delta$  is the following:

$$\delta = \frac{Z_{crust\ init}}{(Z_{Moho\ present} - Z_{basement})} \quad (3)$$

The resulting crustal stretching factors are between ~1 to 2.2 (Fig. 5a), where smaller values indicate almost no thinning of the crust corresponding to areas with no or minor sediment coverage, while highest values are attributed to basinal locations. Subcrustal stretching values cannot be calculated in the same way as the crustal stretching but using the present-day LAB depth, since the base of the lithosphere immediately after extension has considerably changed through post-rift cooling (Lenkey, 1999). Therefore, we selected constant prior values for  $\beta$ , which we updated through the inversion procedure (Section 3.4) to account for its potential spatial variations. We tested several starting values for  $\beta$  between 1.5 to 4, and finally we chose  $\beta=3$ , since this value provided the prior model best fitting to temperature observations. Considering the initial lithosphere thickness of 120 km, and an initial crustal thickness of 35 km,  $\beta=3$  would mean that the thickness of the mantle lithosphere reduced from 85 km to ~ 28 km during rifting. The active rifting phase was followed by post-rift thermal subsidence and corresponding post-rift sedimentation. We incorporated the effect of post-rift sedimentation by assuming constant sedimentation rates between 10 – 0 Ma, based on the thickness of Pannonian (Upper Miocene) and Quaternary sediments (Table 2). Post-rift cooling was incorporated in the model by defining stretching of 1 after the syn-rift period.



225 **Figure 5: (a) Prior crustal stretching ( $\delta$ ) and (b) posterior subcrustal stretching ( $\beta$ ) values representing the extension of the crust and mantle lithosphere. Note that  $\delta$  shown in (a) and  $\beta = 3$  were used as input parameters for the stretching module, and  $\beta$  shown in (b) is the posterior mantle stretching factor resulting from the inversion procedure, conditioned with temperature observations.**

### 3.4 Inversion procedure

We conditioned the thermal model with temperature observations from wells, using a selection of temperature measurements with assigned uncertainties described in Section 3.2. During the data assimilation procedure, the only model parameter we updated was the subcrustal stretching factor  $\beta$ . We selected only  $\beta$  for the model update as we were primarily interested in lithosphere-scale thermal field and thermal evolution. We did not update the shallower part of the model (e.g. thermal parameters of the sediments) since an already good fit with temperature observations was achieved by only modifying  $\beta$ , that is responsible for the large-scale thermal perturbations affecting the model area.

230

To estimate the subcrustal stretching factor ( $\beta$ ), we applied ensemble-based probabilistic inversion. The Ensemble Smoother (ES, Emerick and Reynolds, 2013a) estimates the model parameters by a global update, incorporating all data available. This allows for the solution of inverse problems with large number of observations in a computationally efficient way. For non-linear forward models, the ES requires several iterations, where the prediction of the previous run is used as an input for the subsequent data assimilation step (ES-MDA, Emerick and Reynolds, 2013b).

235

The solution for a single data assimilation for the updated model ensemble is:

$$\hat{M} = M + M'[GM']^T \{GM'[GM']^T + (N_e - 1)C_d^{-1}\}^{-1} \times (D - GM) \quad (4)$$

240 In equation 4,  $M$  is the prior ensemble of model parameters,  $GM$  is the result of the forward model working on all ensemble members, and  $GM'$  is the difference between  $GM$  and its mean.  $N_e$  represents the number of ensembles, and  $D$  is an ensemble of data realizations, created by perturbing the measurements according to their covariance matrix ( $C_d$ ). The mean of the ensemble is taken as the best estimate, which is used as input for the next update in case of ES-MDA. The number of data



assimilation steps,  $N_a$  must be selected a-priori. The data covariances used for the update steps are increased by a multiplication  
245 factor,  $\alpha_i$  for  $i=1,2,\dots, N_a$ , and  $\alpha_i$  must be selected as  $\sum_{i=1}^{N_a} \frac{1}{\alpha_i} = 1$  (Emerick and Reynolds, 2013b). This is necessary to  
compensate for the effect of multiple applications of an ES.

The prior uncertainty in  $\beta$  was taken into account by scaling the initial  $\beta$  values of 3 to a uniform distribution between 2 and  
5. The spatial variability of  $\beta$  was determined through a spherical variogram. The radius of the variogram includes 15 model  
250 cells, which corresponds to  $\sim 45$  km. This relatively large distance was selected because variations in subcrustal stretching were  
considered to be large-scale. During the ES-MDA procedure, we chose 4 iterations, each with 700 model runs (ensembles).  
The resulting  $\beta$  field (Fig. 4b) shows variations between 2.2-3.4, where largest values correspond to the Zala basin, and the  
areas marked by less intense subcrustal stretching are predicted for the NW part of the model area.

## 4 Results

### 4.1 Shallow (0-5 km) temperature field

255 Present-day posterior model temperatures, calculated with the updated subcrustal stretching factors,  $\beta$ , are in general higher in  
basinal areas (Zala basin, Danube basin) and lower in peripheral areas (Transdanubian Range, Sopron Mts.) (Fig. 6.). The  
largest positive thermal anomaly at 2 km depth corresponds to the Zala basin in the SW, reaching up to 110 °C (Fig. 6, left  
panel). The pattern of anomalies at 4 km depth is slightly different: the most pronounced positive anomaly corresponds to the  
Danube basin in the north, with temperatures up to 170 °C, meaning a geothermal gradient of  $\sim 45$  °C/km. Since convection  
260 connected to fluid flow is not considered in the model, the modelled thermal anomalies can be explained with conductive  
thermal effects. Positive anomalies are the reflection of sediment blanketing, meaning the insulating effect of sediments with  
low thermal conductivity. Negative anomalies can be attributed to outcropping/near-surface basement rocks (mostly  
carbonates) having significantly higher thermal conductivities. It is important to note that the conductive thermal modelling  
approach is a valid assumption for the majority of the study area, resulting in realistic predicted temperatures. The conductive  
265 assumption is although not fully valid for parts of the Transdanubian range built up by fractured and karstified carbonate rocks.  
Groundwater flow within the top 5 km alters the conductive regime at these areas, and therefore predicted temperatures cannot  
be considered reliable in the shallow part of the model. Misfits between modelled and observed temperatures do not indicate  
this bias, since temperature measurements affected by fluid flow were excluded from the calibration dataset to properly account  
for the transient effect of lithosphere extension (see section 3.2).



270

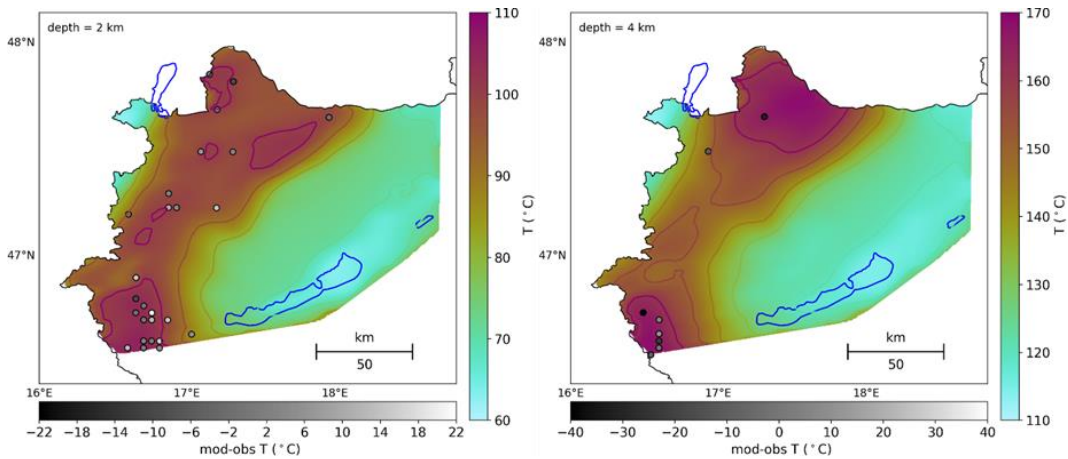


**Figure 6:** (a) Isodepth temperature maps predicted by the present-day posterior model at 2 km (left panel) and 4 km (right panel) depth. The misfits between modelled and observed temperatures are indicated with color-coded circles, within the depth interval of  $\pm 200$  m.

The driving effect of sediment blanketing in shallow (0-5 km) depth is also clearly visible on the temperature-depth profiles (Fig. 7.). Temperatures are significantly higher in basinal profiles (Fig. 7 a, b) than in marginal settings (Fig. 7 c, d). In all cases, the thermal effect of lithosphere extension is clearly visible: temperatures prior to stretching (black lines) are significantly lower than present-day geotherms (blue lines). Modelled present-day temperatures show a generally good fit with observations, although misfits in the deeper ( $> \sim 3.5$  km) exist in both the Danube and Zala basins. Some of these misfits may be explained by measurement errors but may also be attributed to changes in sediment geometry and composition further away from the profile location or can even be caused by local fluid convection e.g. in the carbonate basement (Fig. 7c).

280

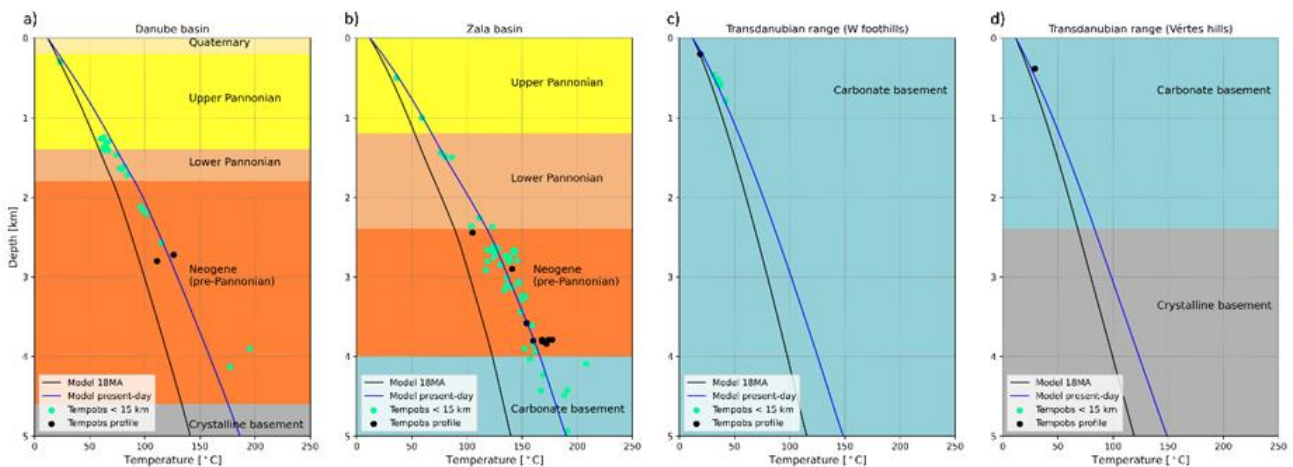


**Figure 7:** Shallow (0-5 km) temperature-depth profiles in the Danube basin (a), Zala basin (b), and from two locations within the Transdanubian Range (c: western foothills, d: Vértes hills). Blue line represents the present-day geotherm, black line shows the



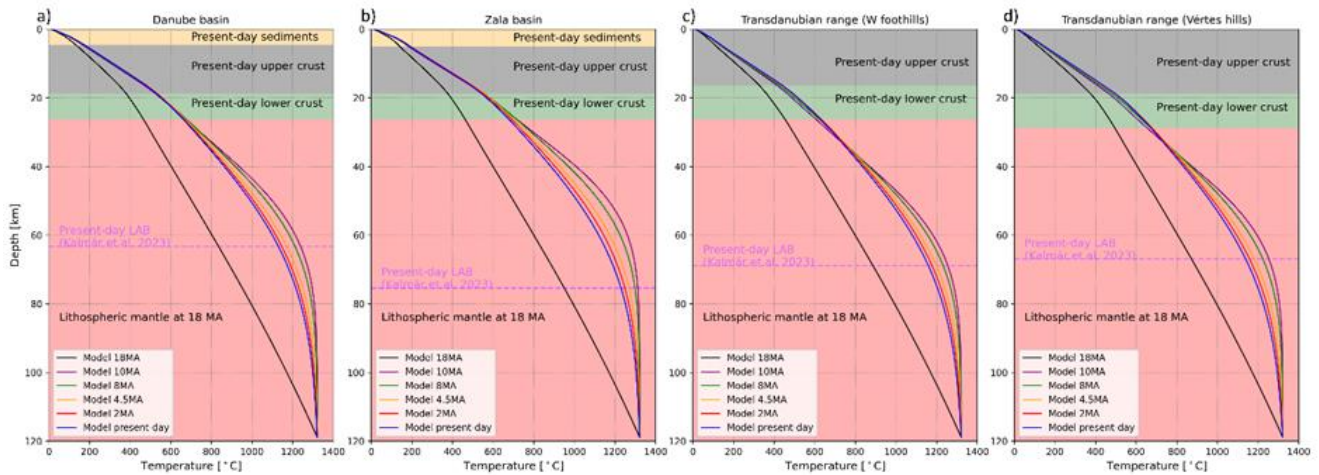
285 **geotherm prior to lithosphere extension. Black circles show temperature measurements from wells at the location of the profile, while green circles indicate measurements from wells within 15 km distance. For the locations of the profiles see Fig. 3.**

#### 4.2. Lithosphere thermal field

The transient thermal field in the whole lithosphere was calculated by stretching the initial thermal model prior to extension (representing the thermal state of the lithosphere at 18 Ma) using crustal ( $\delta$ ) and subcrustal ( $\beta$ ) stretching factors described in section 3.2.  $\beta$  was initially set to a constant value for the prior modelling, then a spatial variation of  $\beta$  was introduced and  $\beta$  values were updated to fit present-day model temperatures to temperature observations (described in detail in section 3.2). The resulting updated  $\beta$  values vary between 2.2 and 3.4 (Fig. 5.), suggesting that more than half of the initial mantle lithosphere was attenuated during extension in the entire area. Posterior  $\beta$  values are the highest in the Zala basin, while  $\beta$  is significantly lower in the Danube basin. This does not necessarily mean that lithosphere thinning was less pronounced but can also be due to the fact that extension in the NW part of the study area happened earlier (ref). Lower predicted  $\beta$  values in the Danube basin can simply mean that the thermal relaxation of the lithosphere is in a more advanced stage here, due to the older main stretching phase.

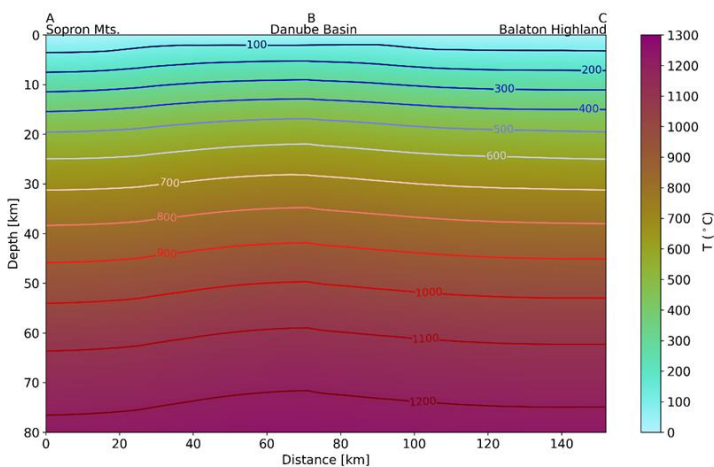
Lithosphere geotherms prior to stretching at 18 Ma (black lines in Fig. 8.) are significantly colder than past extension geotherms. The initial geotherms at 18 Ma indicate variations in geothermal gradient at two major compositional variations (sediment/basement and upper/lower crust boundary) according to the present-day model geometry. This is explained by the fact that present-day upper crustal geometries were used as a primary model input, since this setting provided the most appropriate initial conditions for the stretched models. Since no sediments and a thicker upper crust existed before extension, the initial thermal model representing the temperature field at 18 Ma is slightly biased in upper crustal levels. Going deeper, predicted initial lithosphere temperatures are almost identical for all locations (Fig. 8. a-d), that agrees with expectations that no major lateral temperature variations are expected in the lithosphere at 18 Ma.

We present the modelled thermal field affected by lithosphere extension for various representative time intervals (10 Ma, 8 Ma, 4.5 Ma, 2 Ma, 0 Ma, Fig. 7). All temperature profiles reach 1330 °C at the depth of 120 km associated with the LAB, prescribed as a bottom boundary condition for all models. The actual post stretching LAB is significantly shallower, as suggested by the 10 – 0 Ma geotherms. Highest temperatures in the lithospheric mantle are attributed to the 10 Ma model (purple line in Fig. 8.), representing the thermal state right after extension. 10 – 0 Ma models represent the conductive cooling (thermal relaxation) of the lithosphere. Cooling is combined with the thermal effect of post-rift sedimentation, that is most pronounced at the shallower parts of the models in basinal locations (Fig. 8 a, b). Present-day lithosphere temperature predictions as well as the elevated geothermal gradient and surface heat flow of the area (Lenkey et al., 2002) evidence that the thermal state of the lithosphere has not yet reached steady-state.



315 **Figure 8: Lithosphere temperature-depth profiles in the Danube basin (a), Zala basin (b), and from two locations within the Transdanubian Range (c: western foothills, d: Vértes hills). Color-coded lines represent geotherms from different times between 18 Ma – present. The depth extent of major units is also indicated, together with the present-day LAB (dashed purple line) from Kalmár et al. (2023). For the locations of the profiles see Fig. 3.**

Present-day modelled temperatures are generally (slightly) elevated in basinal areas than the peripheral locations throughout the entire lithosphere (Figs. 8, 9). Higher temperatures in the Danube basin through the temperature profile in Fig. 9 represent the combined effect of lithosphere extension (controlling the thermal field in the mantle lithosphere) and sediment blanketing (having major influence in the crustal thermal field). Towards the Transdanubian Range (Balaton Highland), predicted model temperatures are slightly higher in the deeper part of the model compared to the NW part (Sopron Mts.). This might be explained by the shift in the timing of active rifting, that migrated from NW towards SE (e.g. Balázs et al., 2016).



325



**Figure 9: Lithosphere temperature cross-section representing present-day predicted temperatures from the Sopron Mts. through the Danube basin to the Balaton Highland. For the location of the section see Fig. 3.**

To quantify the added value of the data assimilation procedure through updating the subcrustal stretching factor ( $\beta$ ), we compared the overall misfit between modelled and observed temperatures of the present day prior (no data assimilation,  $\beta=3$ ) and posterior model (data assimilation with spatial variation in  $\beta$ ). Through the data assimilation, the mean misfit has significantly decreased from 1.33 °C to 0.42 °C (Table 3.). The median and RMS of the posterior model also decreased, but less significantly. Positive mean and median values indicate that the models slightly overestimate measured temperatures overall. More significant improvements of the misfit, especially in terms of the RMS where positive and negative errors do not cancel out, could be achieved by updating the thermal properties of the shallower part of the model (e.g. thermal conductivity of sediments, radiogenic heat generation in the upper crust). This exercise was excluded from the current study, as here we focus mainly on lithospheric scale thermal processes and thermal evolution of the lithosphere, which is primarily captured by the crustal and subcrustal stretching factors.

Model type	Mean	Median	RMS
Prior (present-day)	1.33	3.40	1.46
Posterior (present-day)	0.42	2.81	1.43

**Table 3: Mean, median and RMS misfit of the present-day prior and posterior models in °C, calculated using all temperature measurements.**

## 340 5 Discussion

### 5.1 Implications for the thermal evolution of the lithosphere

It has already been shown by Royden et al. (1983) that the elevated heat flow and geothermal gradient in the Pannonian basin can only be explained if the mantle lithosphere attenuation was more pronounced than crustal stretching ( $\beta > \delta$ ). Crustal and subcrustal stretching factors calculated by Lenkey (1999) largely support this finding, while they predict large variations in subcrustal stretching in the study area, extending from  $\beta = 1$  in the Balaton-Highland to  $\beta=3$  in the Zala basin. Predicted subcrustal stretching in this study for the same area represents a much more homogenous picture with  $\beta$  values between 2.2-3.4 (Fig. 5b). Using these factors for mantle lithosphere extension between 18-10 Ma, together with accounting for the thermal effect of sedimentation and changes in upper crustal heat generation, we were able to reproduce present-day temperature observations representing a conductive thermal regime. It must be noted that the predicted subcrustal stretching might not be entirely correct due to changes in the timing of stretching throughout the study area but provide a realistic picture for the degree of lithosphere attenuation.





The moderate lateral variations in modelled past and present-day lithosphere temperatures (Figs. 8, 9) and  $\beta$  field (Fig. 5) suggest that the lateral variations in the past and present-day lithosphere thickness are rather limited in the study area. This agrees with the LAB depth recently inferred from seismological observations (Kalmár et al., 2023), with predictions between  
355 ~60-80 km in the study area (dashed purple lines in Fig. 8 based on Kalmár et al. (2023)). Previous LAB depth maps (Horváth et al., 2006; Tari et al., 1999) infer significantly higher values up to ~105 km in the NW part of the study area, while these were constructed based on limited seismological data derived from lower number of seismic stations compared to Kalmár et al. (2023). Lithosphere scale thermal models of Lenkey et al. (2017) and Békési et al. (2018) building on the previous LAB depth map may therefore predict inaccurate temperatures deep down in the lithosphere in NW Hungary. We compared the  
360 present-day posterior model with one of the temperature models of Békési et al. (2018) incorporating the thermal footprint of extension without actual transient calculations. Lithosphere temperatures below ~ 10 km depth in Békési et al. (2018) are significantly higher than in case of the current model, suggesting that steady model assumptions to mimic transient thermal processes led to the overestimation of deep lithosphere temperatures.

In terms of the shallow (<5 km) temperature field, predicted temperatures in the Danube basin and Zala basin are slightly  
365 higher than those presented in Lenkey et al. (2017) and (Lenkey et al., 2021), while slightly lower than the conductive thermal model predictions in the OGRE database (Ogre, 2020). These differences in shallow temperature predictions can partly be explained by the different calibration datasets used by Lenkey et al. (2017) and (Lenkey et al., 2021), excluding temperature measurements from (recent) geothermal wells documented in the OGRE database. Additionally, higher lithosphere thickness adopted in Lenkey et al. (2017) in the Western periphery of Hungary, discussed in the previous chapter, might be partly  
370 responsible for the lower predicted temperatures also in the shallow sedimentary units. Our thermal model assumes a conductive thermal regime, and therefore cannot be considered reliable at areas where groundwater flow in fractured/karstified carbonates possibly influence/dominate the temperature field. Although, deeper down in the lithosphere, we consider past and present-day conductive temperature predictions realistic.

## 5.2 Rheological inferences of the new thermal model

375 Temperature substantially influences the rheology of the lithosphere, as the ductile strength of rocks is an exponential function of temperature. The transient thermal model presented here is significantly more realistic below ca. 10 km depth with respect to previous models (Békési et al., 2018; Limberger et al., 2018), hence, it allows a more precise evaluation of lithosphere rheology. We estimate the yield stress (maximum differential stress prior to frictional or ductile yielding) of the lithosphere by the combination of Byerlee's law for frictional deformation and dislocation creep flow laws for the upper crust, lower crust,  
380 and mantle (for material-dependent parameters see Table A1). For the upper crust, we use Westerly granite flow law (Hansen and Carter, 1983). For the lower crust, we use a 0.7-0.3 mixture of mafic granulite and dry quartz (Ranalli, 1995) according to the typical composition of the lower crust (Török, 2012). To calculate the material constants of the mixture, we apply the formula of (Tullis et al., 1991). For mantle creep, we use a wet olivine average from Ranalli (1995) and Kirby and Kronenberg



(1987). Strain rate is defined as an average value for NW-Hungary (3 nstrain/yr), based on Porkoláb et al. (2023). For Byerlee's  
385 law, we use a coefficient for compression ( $\mu = 3$ ) based on Ranalli and Murphy (1987), a pore fluid factor for hydrostatic case  
( $\beta = 0.36$ ) and the gravitational acceleration constant ( $g = 9.81 \text{ m/s}^2$ ).

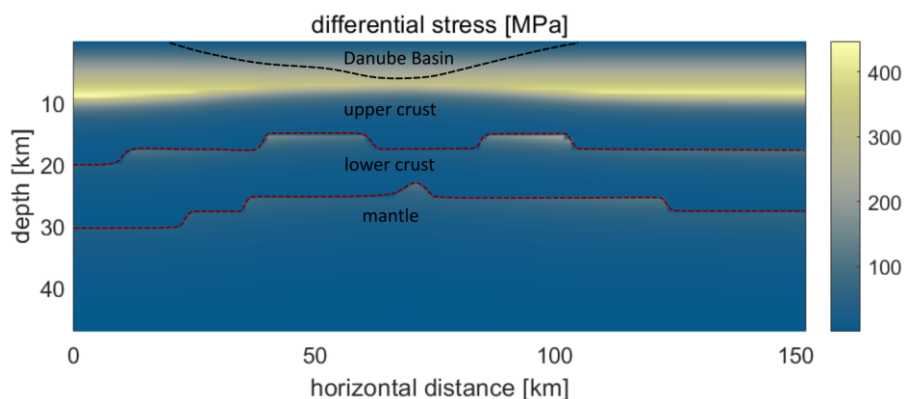


**Figure 10: Differential stress (yield stress) profile from the Sopron Mts. (left) to the Balaton Highland (right, for map-view trace see Fig. 3b). Black dashed line indicates the lower limit of the Danube basin, red dashed lines indicate the Conrad and Moho discontinuities based on Kalmár et al. (2021).**  
390

Results show that most of the lithospheric strength is concentrated in the shallow parts of the upper crust, which is the only brittle layer in the Pannonian lithosphere (Fig. 10). Increased differential stress levels below this shallow upper crust are possible at discontinuities (such as the Conrad and Moho) where lithology and thus viscous creep parameters change. The brittle-ductile transition zone is marked by a sharp decrease in differential stress (Fig. 10) at 7-8 km depth below the Danube basin and 9-10 km at the basin margins (Sopron Mts and Balaton Highland), showing that basins are relatively weaker, and  
395 viscous creep in the upper crust becomes efficient at quite shallow levels due to high temperatures. These rheological estimations agree with the generally shallow, < 12 km depth of earthquake hypocenters in the Pannonian basin (Tóth et al., 2002-2010; Lenkey et al., 2002; Porkoláb et al., under revision; Bondár et al., 2018). For a more detailed analysis and parameter test see Porkoláb et al. (under revision).

### 400 5.3 Geochemical implications

The lithosphere-scale thermal model is of high relevance to decipher the structure of the lower lithosphere via the understanding of the vertical distribution of upper mantle-derived rocks. In areas like the Bakony-Balaton Highland Volcanic Field (BBHVF) in the Balaton Highland (Fig. 1.), where hundreds of xenoliths have been described representing the subcontinental off-cratonic lithospheric mantle, is an ideal example. Over the past 20+ years, extended petrographic,  
405 geochemical and deformation knowledge has been gained via the detailed investigation on these mantle xenoliths from this region (Szabó et al., 2004). Xenoliths have been brought to the surface by intracontinental monogenetic basaltic volcanism between ~8 to 2.6 Ma (Balogh et al., 1986; Balogh and Nemeth, 2005; Wijbrans et al., 2007), thus xenoliths from the same eruption event represent lithospheric mantle portion with the same age than the upbringing volcanism. Considering this,



410 sampled subcontinental mantle lithosphere is available for the time slices of 7.96, 4.53, and 2.61 million years (based on Ar-Ar dating on the pyroclastic rocks by Wijbrans et al. (2007) of Tihany, Szigliget, and Füzés-tó volcanoes, respectively), similar to the ages to of the thermal models in this study.

Subcontinental lithospheric mantle, stable between Moho and LAB discontinuities, mainly consists of Mg-Fe-Ca silicates like olivine, ortho- and clinopyroxene. In addition to the silicates, Al-bearing phases such as garnet and spinel yield the rock stability at higher and lower pressure (depth), respectively. In the study area, as a result of the extremely thinned sampled continental lithosphere, only spinel-bearing rocks (lherzolites) have been documented among the mantle-derived xenoliths. For the garnet-bearing mantle xenoliths (sampled at rather cratonic lithospheric portions), mineral chemistry-based pressure (depth)-temperature relations of the lithospheric mantle can be applied to understand the structure of the mantle lithosphere (O'reilly and Griffin, 2010). In contrast, for the spinel lherzolite-type rocks, only temperature calibration can be used based on orthopyroxene-clinopyroxene mineral equilibrium (Brey and Köhler, 1990) owing to the lack of any geochemistry-based pressure or depth estimation. The equilibrium temperature of BBHVF mantle xenoliths is between 880 and  $1160 \pm 16$  °C (Szabó et al., 2004).

The temperature model provided in this study can overcome this issue by the fruitful interdisciplinary application of petrologic, geochemical and geophysical tools. This approach may give plausible estimation for the depth of origin of the mantle xenoliths. It is important as the question whether or not the mantle xenoliths derive from specific depth(s) or are well distributed for the entire mantle lithosphere remains unanswered for most of the mantle xenolith locations worldwide. Sampling depths of mantle xenoliths from the study area were calculated by crossing of the suitable geotherm (i.e., model age of the thermal model and volcanic eruption age should be the closest possible) with the isotherm derived from the aforementioned mineral equilibrium. Using these data, the following sampling depth range were provided: Tihany - 41-61 km (23 sample; sampling age and thermal model age: 7.96 and 8.00 Ma, respectively), Szigliget - 39-66 km (25 sample; 4.53 and 4.00 Ma) and Füzés-tó - 36-70 km (72 sample; 2.61 and 2.00 Ma). It is noteworthy to mention that depth ranges show continuous distribution between the shallowest and deepest depths. Approximating from present-day Moho and LAB depth of the study area (Kalmár et al., 2023), we can thus state that most of the mantle lithosphere has been vertically sampled in the tested three time slices. In other words, using the new thermal model on mantle xenolith datasets, we could test and confirm their representativity for the mantle lithosphere volumes.

## 435 **6 Conclusions**

The presented methodology of incorporating transient thermal effects, using crustal and subcrustal stretching factors, and accounting for sedimentation proved successful in reproducing the most important thermal footprints of basin evolution. The extension of the forward model with the data assimilation workflow to condition the model with temperature observations provided quantitative measures for the reliability of the models and allowed to constrain model parameters. Past and present-day temperature predictions for NW-Hungary can be considered realistic within the whole lithosphere, in contrast with



previous models where deep lithospheric temperatures were relatively imprecise. The calculated crustal and estimated subcrustal stretching values indicate that 1) subcrustal stretching was indeed much more important than crustal stretching in the Pannonian basin: at least half of the mantle lithosphere through the study area was attenuated; 2) subcrustal stretching affected the study area with relatively similar degrees compared to crustal stretching, the crust at several marginal areas remained (almost) intact while crustal thickness under basins decreased to more than half of the assumed pre-stretching setting. These findings generally agree with expectations such as the rise of the asthenosphere translates to larger-scale ductile deformation of the lower part of the lithosphere, while the extension through faulting in the brittle (upper) crust is more localised. Additionally, the predicted present-day lithosphere temperatures suggest that the depth of the current LAB is relatively homogenous, supporting the new seismological model of Kalmár et al., 2023. The new temperature model allows the improved estimation of lithosphere rheology and the origin of mantle xenoliths over the Balaton Highland. The presented methodology can be adopted and applied to model the thermal evolution of sedimentary basins worldwide. The resulting past- and present-day temperature predictions can further be used to constrain geodynamic processes of the study area and provide first-order input for geothermal exploration.

## Appendix

455

	sediments	upper crust	lower crust	mantle
$\rho$ , density [ $\text{kg/m}^3$ ]	2500	2650	2850	3300
$n$ , power law exponent [-]		3.3	3.55	4
$E$ , activation energy [kJ]		186.5	340.8	471
$A$ , pre-exponential constant [ $\text{Pa}^{-n} \cdot \text{s}^{-1}$ ]		$3.16 \cdot 10^{-26}$	$3.01 \cdot 10^{-21}$	$2 \cdot 10^{-21}$

**Table A1. Material properties for differential stress (yield stress) calculations (Fig. 7). Upper crust and sediments: Westerly granite (Hansen and Carter, 1983). Lower crust: 0.7-0.3 mixture of mafic granulite and dry quartz (Ranalli, 1995) Mantle: wet olivine average from Ranalli (1995) and Kirby and Kronenberg (1987).**

## 460 Data Availability

Temperature models have been deposited in Mendeley with the primary accession link <https://data.mendeley.com/drafts/vp7jdp79y4>.



### Author contributions

**Eszter Békési:** Conceptualization; Investigation; Methodology; Validation; Visualization; Writing - original draft; Writing - review & editing; **Jan-Diederik van Wees:** Conceptualization; Methodology; Resources; Software; Supervision; Validation; Roles - original draft; Writing - review & editing; **Kristóf Porkoláb:** Conceptualization; Visualization; Roles - original draft; Writing - review & editing; **Mátyás Hencz:** Writing - review & editing, **Márta Berkesi:** Conceptualization; Investigation; Project administration; Resources; Roles - original draft; Writing - review & editing

### Competing interest

470 The authors declare that they have no conflict of interest.

### Acknowledgements

The reported investigation was financially supported by the MTA FI FluidsByDepth Lendület (Momentum) project, provided by the Hungarian Academy of Sciences (grant nr. LP2022-2/2022) and by the National Research, Development and Innovation Fund, Hungary under grant number PD147116. Figures were created with Qgis, Inkscape and Python, using the scientific colour maps (when applicable) of Fabio Crameri (<http://doi.org/10.5281/zenodo.1243862>).

### References

- Bada, G., Horváth, F., Dövényi, P., Szafián, P., Windhoffer, G., and Cloetingh, S.: Present-day stress field and tectonic inversion in the Pannonian basin, *Global and Planetary Change*, 58, 165-180, 2007.
- 480 Balázs, A., Matenco, L., Magyar, I., Horváth, F., and Cloetingh, S.: The link between tectonics and sedimentation in back-arc basins: New genetic constraints from the analysis of the Pannonian Basin, *Tectonics*, 35, 1526-1559, <https://doi.org/10.1002/2015TC004109>, 2016.
- Balogh, K. and Nemeth, K.: Evidence for the neogene small-volume intracontinental volcanism in western Hungary: K/Ar geochronology of the Tihany Maar volcanic complex, 2005.
- 485 Balogh, K., Árva-Sós, E., Pécskay, Z., and Ravasz-Baranyai, L.: K/Ar dating of post-sarmatian alkali basaltic rocks in Hungary, *Acta Mineralogica Petrographica*, 27, 75-93, 1986.
- Békési, E., Porkoláb, K., Wertzger, V., and Wéber, Z.: Updated stress dataset of the Circum-Pannonian region: Implications for regional tectonics and geo-energy applications, *Tectonophysics*, 856, 229860, <https://doi.org/10.1016/j.tecto.2023.229860>, 2023.
- 490 Békési, E., Struijk, M., Bonté, D., Veldkamp, H., Limberger, J., Fokker, P. A., Vrijlandt, M., and van Wees, J.-D.: An updated geothermal model of the Dutch subsurface based on inversion of temperature data, *Geothermics*, 88, 101880, <https://doi.org/10.1016/j.geothermics.2020.101880>, 2020.
- Békési, E., Lenkey, L., Limberger, J., Porkoláb, K., Balázs, A., Bonté, D., Vrijlandt, M., Horváth, F., Cloetingh, S., and van Wees, J.-D.: Subsurface temperature model of the Hungarian part of the Pannonian Basin, *Global and Planetary Change*, 171, 48-64, <https://doi.org/10.1016/j.gloplacha.2017.09.020>, 2018.
- 495 Bondár, I., Mónus, P., Czanik, C., Kiszely, M., Grácz, Z., and Wéber, Z.: Relocation of seismicity in the Pannonian basin using a global 3D velocity model, *Seismological Research Letters*, 89, 2284-2293, <https://doi.org/10.1785/0220180143>, 2018.



- Bonté, D., Van Wees, J.-D., and Verweij, J.: Subsurface temperature of the onshore Netherlands: new temperature dataset and modelling, *Netherlands Journal of Geosciences*, 91, 491-515, <https://doi.org/10.1017/S001677460000354>, 2012.
- 500 Brey, G. P. and Köhler, T.: Geothermobarometry in four-phase lherzolites II. New thermobarometers, and practical assessment of existing thermobarometers, *Journal of Petrology*, 31, 1353-1378, 1990.
- Buck, W. R., Martinez, F., Steckler, M. S., and Cochran, J. R.: Thermal consequences of lithospheric extension: pure and simple, *Tectonics*, 7, 213-234, 1988.
- Budai, T., Császár, G., Csillag, G., Dudko, A., Koloszar, L., and Majoros, G.: A Balaton-felvidék földtana, Térkép és magyarázó [The geology of Balaton Highland, Map and explanation], *Periodical Hungarian Geol Institute*, 197:257, 1999.
- 505 Chapman, D.: Thermal gradients in the continental crust, *Geological Society, London, Special Publications*, 24, 63-70, <https://doi.org/10.1144/GSL.SP.1986.024.01.07>, 1986.
- Corver, M. P., Doust, H., van Wees, J. D., Bada, G., and Cloetingh, S.: Classification of rifted sedimentary basins of the Pannonian Basin System according to the structural genesis, evolutionary history and hydrocarbon maturation zones, *Marine and Petroleum Geology*, 26, 1452-1464, <https://doi.org/10.1016/j.marpetgeo.2008.12.001>, 2009.
- 510 Danielson, J. J. and Gesch, D. B.: Global multi-resolution terrain elevation data 2010 (GMTED2010), 2011.
- Dövényi, P. and Horváth, F.: A Review of Temperature, Thermal Conductivity, and Heat Flow Data for the Pannonian Basin: Chapter 16, <https://doi.org/10.1306/M45474C16>, 1988.
- Dövényi, P., Horváth, F., and Drahos, D.: Geothermal thermic map (Hungary), *Atlas of geothermal resources in Europe. Office for Official Publications of the European Communities (Luxembourg)*, 267, 2002.
- 515 Emerick, A. A. and Reynolds, A. C.: Investigation of the sampling performance of ensemble-based methods with a simple reservoir model, *Computational Geosciences*, 17, 325-350, <https://doi.org/10.1007/s10596-012-9333-z>, 2013a.
- Emerick, A. A. and Reynolds, A. C.: Ensemble smoother with multiple data assimilation, *Computers & Geosciences*, 55, 3-15, <https://doi.org/10.1016/j.cageo.2012.03.011>, 2013b.
- Farr, T. G., Rosen, P. A., Caro, E., Crippen, R., Duren, R., Hensley, S., Koberick, M., Paller, M., Rodriguez, E., and Roth, L.: The shuttle radar topography mission, *Reviews of geophysics*, 45, 2007.
- 520 Fodor, L., Bada, G., Csillag, G., Horváth, E., Ruszkiczay-Rüdiger, Z., Palotás, K., Síkhegyi, F., Timár, G., Cloetingh, S., and Horváth, F.: An outline of neotectonic structures and morphotectonics of the western and central Pannonian Basin, *Tectonophysics*, 410, 15-41, <https://doi.org/10.1016/j.tecto.2005.06.008>, 2005.
- Fodor, L., Balázs, A., Csillag, G., Dunkl, I., Héja, G., Jelen, B., Kelemen, P., Kövér, S., Németh, A., and Nyíri, D.: Crustal exhumation and depocenter migration from the Alpine orogenic margin towards the Pannonian extensional back-arc basin controlled by inheritance, *Global and Planetary Change*, 201, 103475, <https://doi.org/10.1016/j.gloplacha.2021.103475>, 2021.
- 525 Goutorbe, B., Lucazeau, F., and Bonneville, A.: Comparison of several BHT correction methods: a case study on an Australian data set, *Geophysical Journal International*, 170, 913-922, <https://doi.org/10.1111/j.1365-246X.2007.03403.x>, 2007.
- Grenerczy, G., Sella, G., Stein, S., and Kenyeres, A.: Tectonic implications of the GPS velocity field in the northern Adriatic region, *Geophysical Research Letters*, 32, <https://doi.org/10.1029/2005GL022947>, 2005.
- 530 Haas, J., Budai, T., Csontos, L., Fodor, L., Konrád, G., and Koroknai, B.: Geology of the pre-Cenozoic basement of Hungary, *Geological and Geophysical Institute of Hungary, Budapest*, 1-71, 2014.
- Hansen, F. and Carter, N.: Semibrittle creep of dry and wet Westerly granite at 1000 MPa, *ARMA US Rock Mechanics/Geomechanics Symposium*, ARMA-83-0429, 1983.
- 535 Hantschel, T. and Kauerauf, A. I.: *Fundamentals of basin and petroleum systems modeling*, Springer Science & Business Media 2009.
- Héja, G., Ortner, H., Fodor, L., Németh, A., and Kövér, S.: Modes of oblique inversion: A case study from the Cretaceous fold and thrust belt of the western Transdanubian Range (TR), West Hungary, *Tectonics*, 41, e2021TC006728, <https://doi.org/10.1029/2021TC006728>, 2022.
- 540 Hetényi, G. and Bus, Z.: Shear wave velocity and crustal thickness in the Pannonian Basin from receiver function inversions at four permanent stations in Hungary, *Journal of seismology*, 11, 405-414, <https://doi.org/10.1007/s10950-007-9060-4>, 2007.
- Horváth, F. and Cloetingh, S.: Stress-induced late stage subsidence anomalies in the Pannonian Basin, *Tectonophysics*, 266, 287-300, [https://doi.org/10.1016/S0040-1951\(96\)00194-1](https://doi.org/10.1016/S0040-1951(96)00194-1), 1996.
- 545 Horváth, F., Bada, G., Szafián, P., Tari, G., Ádám, A., and Cloetingh, S.: Formation and deformation of the Pannonian Basin: constraints from observational data, *Geological Society, London, Memoirs*, 32, 191-206, <https://doi.org/10.1144/GSL.MEM.2006.032.01.11>, 2006.



- Horváth, F., Musitz, B., Balázs, A., Végh, A., Uhrin, A., Nádor, A., Koroknai, B., Pap, N., Tóth, T., and Wórum, G.: Evolution of the Pannonian basin and its geothermal resources, *Geothermics*, 53, 328-352, <https://doi.org/10.1016/j.geothermics.2014.07.009>, 2015.
- 550 Kalmár, D., Hetényi, G., Balázs, A., Bondár, I., and Group, A. W.: Crustal thinning from orogen to back-arc basin: The structure of the Pannonian Basin region revealed by P-to-S converted seismic waves, *Journal of Geophysical Research: Solid Earth*, 126, e2020JB021309, <https://doi.org/10.1029/2020JB021309>, 2021.
- Kalmár, D., Petrescu, L., Stipčević, J., Balázs, A., János Kovács, I., AlpArray, and Groups, P. W.: Lithospheric Structure of the Circum-Pannonian Region Imaged by S-To-P Receiver Functions, *Geochemistry, Geophysics, Geosystems*, 24, e2023GC010937, <https://doi.org/10.1029/2023GC010937>, 2023.
- 555 Kilenyi, E. and Šefara, J.: Pre-Tertiary basement contour map of the Carpathian Basin beneath Austria, Czechoslovakia and Hungary, *Eötvös Lóránd Geophys. Inst*, Budapest, Hungary, 1989.
- Kirby, S. and Kronenberg, A.: Rheology of the lithosphere: Selected topics, *Reviews of Geophysics*, 25, 1219-1244, 1987.
- 560 Lenkey, L.: Geothermics of the Pannonian basin and its bearing on the tectonics of basin evolution., PhD thesis, Vrije Universiteit, Amsterdam, 215, 1999.
- Lenkey, L., Mihályka, J., and Paróczy, P.: Review of geothermal conditions of Hungary, *Földtani Közöny*, 151, 65-65, 2021.
- Lenkey, L., Dövényi, P., Horváth, F., and Cloetingh, S.: Geothermics of the Pannonian basin and its bearing on the neotectonics, *EGU Stephan Mueller Special Publication Series*, 3, 29-40, <https://doi.org/10.5194/smsps-3-29-2002>, 2002.
- 565 Lenkey, L., Raáb, D., Goetzl, G., Lapanje, A., Nádor, A., Rajver, D., Rotár-Szalkai, Á., Svasta, J., and Zekiri, F.: Lithospheric scale 3D thermal model of the Alpine–Pannonian transition zone, *Acta Geodaetica et Geophysica*, 52, 161-182, <https://doi.org/10.1007/s40328-017-0194-8>, 2017.
- Limberger, J., van Wees, J.-D., Tesauro, M., Smit, J., Bonté, D., Békési, E., Pluymaekers, M., Struijk, M., Vrijlandt, M., Beekman, F., and Cloetingh, S.: Refining the thermal structure of the European lithosphere by inversion of subsurface temperature data, *Global and Planetary Change*, 171, 18-47, <https://doi.org/10.1016/j.gloplacha.2018.07.009>, 2018.
- 570 Mádl-Szőnyi, J. and Tóth, Á.: Basin-scale conceptual groundwater flow model for an unconfined and confined thick carbonate region, *Hydrogeology Journal*, 23, 1359-1380, <https://doi.org/10.1007/s10040-015-1274-x>, 2015.
- O'Kenzie, D.: Some remarks on the development of sedimentary basins, *Earth and Planetary science letters*, 40, 25-32, 1978.
- O'Reilly, S. Y. and Griffin, W.: The continental lithosphere–asthenosphere boundary: can we sample it?, *Lithos*, 120, 1-13, <https://doi.org/10.1016/j.lithos.2010.03.016>, 2010.
- 575 OGRE: Geothermal Information System, MBFSZ, <https://map.mbfisz.gov.hu/ogre/2020>.
- Petersen, K., Armitage, J., Nielsen, S., and Thybo, H.: Mantle temperature as a control on the time scale of thermal evolution of extensional basins, *Earth and Planetary Science Letters*, 409, 61-70, <https://doi.org/10.1016/j.epsl.2014.10.043>, 2015.
- Porkoláb, K., Broerse, T., Kenyeres, A., Békési, E., Tóth, S., Magyar, B., and Wetztergom, V.: Active tectonics of the Circum-Pannonian region in the light of updated GNSS network data, *Acta Geodaetica et Geophysica*, 1-25, 2023.
- 580 Porkoláb, K., Békési, E., Györi, E., Broerse, T., Czece, B., Kenyeres, A., Tari, G., and Wéber, Z.: Present-day stress field, strain rate field and seismicity of the Pannonian Basin: overview and integrated analysis, under revision.
- Ranalli, G.: *Rheology of the Earth*, Springer Science & Business Media 1995.
- Ranalli, G. and Murphy, D. C.: Rheological stratification of the lithosphere, *Tectonophysics*, 132, 281-295, 1987.
- 585 Royden, L. and Keen, C.: Rifting process and thermal evolution of the continental margin of eastern Canada determined from subsidence curves, *Earth and Planetary Science Letters*, 51, 343-361, [https://doi.org/10.1016/0012-821X\(80\)90216-2](https://doi.org/10.1016/0012-821X(80)90216-2), 1980.
- Royden, L., Horváth, F., Nagymarosy, A., and Stegena, L.: Evolution of the Pannonian basin system: 2. Subsidence and thermal history, *Tectonics*, 2, 91-137, <https://doi.org/10.1029/TC002i001p00091>, 1983.
- Schatz, J. F. and Simmons, G.: Thermal conductivity of earth materials at high temperatures, *Journal of Geophysical Research*, 77, 6966-6983, <https://doi.org/10.1029/JB077i035p06966>, 1972.
- 590 Schmid, S. M., Bernoulli, D., Fügenschuh, B., Matenco, L., Schefer, S., Schuster, R., Tischler, M., and Ustaszewski, K.: The Alpine-Carpathian-Dinaridic orogenic system: correlation and evolution of tectonic units, *Swiss Journal of Geosciences*, 101, 139-183, <https://doi.org/10.1007/s00015-008-1247-3>, 2008.
- Šujan, M., Rybár, S., Kováč, M., Bielik, M., Majcin, D., Minár, J., Plašienka, D., Nováková, P., and Kotulová, J.: The polyphase rifting and inversion of the Danube Basin revised, *Global and Planetary Change*, 196, 103375, <https://doi.org/10.1016/j.gloplacha.2020.103375>, 2021.
- 595



- Szabó, C., Falus, G., Zajacz, Z., Kovács, I., and Bali, E.: Composition and evolution of lithosphere beneath the Carpathian–Pannonian Region: a review, *Tectonophysics*, 393, 119-137, <https://doi.org/10.1016/j.tecto.2004.07.031>, 2004.
- Szafián, P., Tari, G., Horváth, F., and Cloetingh, S.: Crustal structure of the Alpine–Pannonian transition zone: a combined seismic and gravity study, *International Journal of Earth Sciences*, 88, 98-110, <https://doi.org/10.1007/s005310050248>, 1999.
- 600 Tari, G., Arbouille, D., Schlöder, Z., and Tóth, T.: Inversion tectonics: a brief petroleum industry perspective, *Solid Earth*, 11, 1865-1889, <https://doi.org/10.5194/se-11-1865-2020>, 2020.
- Tari, G., Dövényi, P., Dunkl, I., Horváth, F., Lenkey, L., Stefanescu, M., Szafián, P., and Tóth, T.: Lithospheric structure of the Pannonian basin derived from seismic, gravity and geothermal data, Geological Society, London, Special Publications, 156, 215-250, <https://doi.org/10.1144/GSL.SP.1999.156.01.12>, 1999.
- 605 Tari, G., Bada, G., Beidinger, A., Csizmeg, J., Danišik, M., Gjerazi, I., Grasemann, B., Kováč, M., Plašienka, D., and Šujan, M.: The connection between the Alps and the Carpathians beneath the Pannonian Basin: Selective reactivation of Alpine nappe contacts during Miocene extension, *Global and Planetary Change*, 197, 103401, <https://doi.org/10.1016/j.gloplacha.2020.103401>, 2021.
- Tari, G. C.: Alpine tectonics of the Pannonian Basin, Rice University 1994.
- 610 Tóth, Á., Baják, P., Szijártó, M., Tiljander, M., Korkka-Niemi, K., Hendriksson, N., and Mádl-Szőnyi, J.: Multimethodological Revisit of the Surface Water and Groundwater Interaction in the Balaton Highland Region—Implications for the Overlooked Groundwater Component of Lake Balaton, Hungary, *Water*, 15, 1006, <https://doi.org/10.3390/w15061006>, 2023.
- Tóth, L., Mónus, P., Kiszely, M., and Trosits, D.: Hungarian Earthquake Bulletin, 2002-2010.
- Török, K.: On the origin and fluid content of some rare crustal xenoliths and their bearing on the structure and evolution of the crust beneath the Bakony–Balaton Highland Volcanic Field (W-Hungary), *International Journal of Earth Sciences*, 101, 1581-1597, <https://doi.org/10.1007/s00531-011-0743-2>, 2012.
- 615 Tullis, T. E., Horowitz, F. G., and Tullis, J.: Flow laws of polyphase aggregates from end-member flow laws, *Journal of Geophysical Research: Solid Earth*, 96, 8081-8096, <https://doi.org/10.1029/90JB02491>, 1991.
- Van Wees, J., Van Bergen, F., David, P., Nepveu, M., Beekman, F., Cloetingh, S., and Bonté, D.: Probabilistic tectonic heat flow modeling for basin maturation: Assessment method and applications, *Marine and Petroleum Geology*, 26, 536-551, <https://doi.org/10.1016/j.marpetgeo.2009.01.020>, 2009.
- Wijbrans, J., Németh, K., Martin, U., and Balogh, K.: 40Ar/39Ar geochronology of Neogene phreatomagmatic volcanism in the western Pannonian Basin, Hungary, *Journal of Volcanology and Geothermal Research*, 164, 193-204, <https://doi.org/10.1016/j.jvolgeores.2007.05.009>, 2007.
- 625 Xie, X. and Heller, P. L.: Plate tectonics and basin subsidence history, *Geological Society of America Bulletin*, 121, 55-64, <https://doi.org/10.1130/B26398.1>, 2009.
- Xu, Y., Shankland, T. J., Linhardt, S., Rubie, D. C., Langenhorst, F., and Klasinski, K.: Thermal diffusivity and conductivity of olivine, wadsleyite and ringwoodite to 20 GPa and 1373 K, *Physics of the Earth and Planetary Interiors*, 143, 321-336, <https://doi.org/10.1016/j.pepi.2004.03.005>, 2004.
- 630